Monitoring the temperature dependent elastic and anelastic properties in isotropic polycrystalline ice using resonant ultrasound spectroscopy

Matthew J. Vaughan[1], Kasper van Wijk[2], David J. Prior[1], and M. Hamish Bowman[1]

[1]Department of Geology, University of Otago, 360 Leith Walk, Dunedin, New Zealand, 9054.
[2]Department of Physics, Building 303, University of Auckland, 38 Princes Street, Auckland, New Zealand, 92019

Correspondence to: Matthew Vaughan (mattvaughan902@gmail.com)

Abstract.

The elastic and anelastic properties of ice are of interest in the study of the dynamics of sea ice, glaciers and ice sheets. Resonant ultrasound spectroscopy allows quantitative estimates of these properties and aids calibration of active and passive seismic data gathered in the field. The elastic constants and attenuation constant in man-made polycrystalline isotropic ice

5 cores decrease (reversibly) with increasing temperature. All elastic properties and attenuation vary with ice temperature, but especially compressional-wave speed and attenuation prove sensitive to temperature, indicative of pre-melting of the ice. This method of resonant ultrasound can be deployed in the field, for those situations where shipping samples is difficult (e.g. remote locations), or where the properties of ice change rapidly after extraction (e.g., in the case of sea ice)

1 Introduction

10 Ice sheets flow through a combination of internal deformation and sliding at the base of the ice. The rate of internal deformation is strongly dependent on the englacial temperature, with flow rates increasing for warmer ice. The thermal regime in an ice body controls the onset of basal melting, greatly increasing basal sliding rates and therefore bulk velocity (Hooke et al., 1980; Peters et al., 2012). Ice creep rate is exponentially dependent on temperature (Durham et al., 2010). An englacial temperature uncertainty of 5°C corresponds to an uncertainty in internal deformation rates of a factor of two to five (using activation

15 enthalpies for ice sheets Cuffey and Paterson (2010)). For frozen base scenarios (such as parts of Antarctica), the uncertainties on basal sliding rates that correspond to uncertainty on basal temperature will be of the same order of magnitude. Modelling techniques (Pattyn, 2010; Liefferinge and Pattyn, 2013) have been used to estimate the regional distribution of en-glacial temperature in large ice masses, but thermal profiles of ice sheets from bore holes are extremely limited, and come mainly from ice divides, with few observations from faster flowing ice (Peters et al., 2012). Englacial and basal temperatures across

20 the vast majority of the Antarctic ice sheet are subject to uncertainties on the order of several degrees Celcius, limiting our ability to accurately model the contributions of internal deformation and basal sliding to ice sheet flow. Elsewhere, geophysical methods (ice-penetrating radar and active-source seismology) can provide data on internal structure and physical properties of ice.

Seismic investigations of ice sheets (among others Bentley and Kohnen (1976); Horgan et al. (2011, 2008); Picotti et al. (2015)) present a potential window into the regional scale characteristics of ice bodies. Much focus has recently been placed on understanding the physical properties of ice that influence seismic wave propagation (Maurel et al., 2015). Of particular interest are the relationships of seismic wave attenuation (Peters et al., 2012; Gusmeroli et al., 2010, 2012) to the ice temperature.

5   Wave attenuation from tidal (< 1 Hz) to ultrasonic frequencies (> 20 kHz) in ice exhibits a strong sensitivity to temperature, particularly at high homologous temperatures close to the melting point (Matsushima et al., 2008). In warmer glacial environments such as mountain glaciers and the outlet ice streams of Western Antarctica, variation in attenuation (internal friction) is dominated by energy dissipation in grain boundary processes (Gribb and Cooper, 1998; Jackson et al., 2002; Kuroiwa and Yamaji, 1959; McCarthy et al., 2011) and is thus strongly controlled by the density and the nature of grain boundaries, partic-

10   ularly grain boundary diffusivity. Ice undergoes pre-melting where water (or some modified form of water) exists on ice grain boundaries at temperatures as low as $-30°$C (Hobbs, 1974) when ice creep and grain growth kinetics change radically (Duval et al., 1983). Antarctic ice-sheet thermal structures at ice divides (Engelhardt, 2004) show that the upper ice sheet is below pre-melt temperatures and the base is above pre-melt temperatures, imparting a strong mechanical contrast.

Laboratory measurements of the elastic and anelastic properties of materials can be used to calibrate and understand seis-

15 mic field measurements (Watson and van Wijk, 2015). Here, we use resonant ultrasound spectroscopy (RUS) and time of flight ultrasound measurements to determine the dependence of the elastic and anelastic properties of polycrystalline ice on temperature.

The properties of elastic media can be represented by a stiffness tensor (c_{ijkl}) which relates the stress (σ_{ij}) applied to a sample with the resultant strain (ϵ_{kl}):

$$\sigma_{ij} = c_{ijkl}\epsilon_{kl}, \tag{1}$$

20 which reduces to

$$\sigma_\alpha = c_{\alpha\beta}\epsilon_\beta, \tag{2}$$

when the Voigt recipe is applied (Watson and van Wijk, 2015). For elastically isotropic materials, the stiffness tensor can be reduced to two independent components and expressed as:

$$
\begin{pmatrix}
\sigma_{11} \\
\sigma_{22} \\
\sigma_{33} \\
\sigma_{23} \\
\sigma_{13} \\
\sigma_{12}
\end{pmatrix}
=
\begin{pmatrix}
\lambda+2\mu & \lambda & \lambda & 0 & 0 & 0 \\
\lambda & \lambda+2\mu & \lambda & 0 & 0 & 0 \\
\lambda & \lambda & \lambda+2\mu & 0 & 0 & 0 \\
0 & 0 & 0 & \mu & 0 & 0 \\
0 & 0 & 0 & 0 & \mu & 0 \\
0 & 0 & 0 & 0 & 0 & \mu
\end{pmatrix}
\begin{pmatrix}
\epsilon_{11} \\
\epsilon_{22} \\
\epsilon_{33} \\
2\epsilon_{23} \\
2\epsilon_{13} \\
2\epsilon_{12}
\end{pmatrix},
\tag{3}
$$

where λ and μ are the Lamé constants that define, together with density ρ, the isotropic P- and S-wave velocities as

$$V_p = \sqrt{\frac{\lambda + 2\mu}{\rho}}, \qquad V_s = \sqrt{\frac{\mu}{\rho}}. \tag{4}$$

1.1 Forward modelling

The forward problem is to calculate the mechanical resonance frequencies of an elastic body for a given stiffness tensor, sample geometry, and density. In resonant experiments, sinusoidal excitation is applied to a sample at some point and its measured response is observed at some other point. Using the variational Rayleigh-Ritz method, we can calculate the displacement response of a sample to a sinusoidal point force applied at a particular location as a function of frequency (see Zadler et al. (2004) for a derivation of this relationship).

1.2 The inverse problem

The inverse problem is to estimate the elastic properties of a sample, given the measured resonant frequencies, dimensions, and density. An iterative Levenberg-Marquardt inversion method (Watson and van Wijk, 2015) adjusts the model parameters (the components of $c_{\alpha\beta}$) in order to minimize the difference between measured (f^m) and predicted (f^p) resonant frequencies in a least square sense. We calculate χ^2 values to determine the goodness-of-fit of an isotropic model to our data by the relationship

$$\chi^2 = \frac{1}{N} \sum_i^N w_i \left(\frac{f_i{}^m - f^p}{\sigma_i{}^d} \right)^2, \tag{5}$$

where N is the number of measured modes, σ^d is the estimated uncertainty in the repeatability of each measured mode, and w_i is the weight given to each mode as a measure of the confidence (from 0 to 1) (Watson and van Wijk, 2015). We minimise χ^2 for all our inversions to a narrow level of tolerance (10 - 12) to improve the comparability of our measurements. Starting values of $c_{\alpha\beta}$ for polycrystalline ice are taken from Gammon et al. (1983), and Gusmeroli et al. (2012).

1.3 Anelasticity

The quality factor Q is a frequency-dependent measure of how rapidly wave energy is dissipated due to internal friction in the medium:

$$Q = 2\pi E / \Delta E = f_0 / \delta f, \tag{6}$$

where E is the energy in the wave field, ΔE is the energy lost per cycle due to imperfections in the elasticity in the material, f_0 is the resonant frequency and δf is the full peak width at half maximum amplitude (see box 5.7 in Aki and Richards, 2002). Because RUS operates in the frequency domain capturing all the internally scattered energy at the receiver (Watson and van Wijk, 2015), Q estimates derived from RUS are due to intrinsic attenuation alone.

2   Experimental setup

Ice is prepared using the "standard ice" method (Stern et al., 1997). Samples with a homogeneous foam texture (Fig. 1), a grain size of <1 cm, a random crystallographic preferred orientation (CPO), and nearly isotropic velocity characteristics is frozen in a cylindrical mould (70 mm internal diameter), and machined to 130 mm in length. The sample average density is 0.90 g/cm^3. We

5   estimate the resulting ice sample has $< 2\,\%$ porosity in pores of $< 100\,\mu$m size. Characterising the entire sample microstructure is not practical due its size. It is possible that the sample contains micro-porosity with a non-homogeneous distribution, which may give rise to some anisotropy.

RUS experiments are performed in the setup depicted in Fig. 2, using a contact method outlined in Watson and van Wijk (2015). A function generator (Stanford Research Systems, DS345) sends a swept sinusoidal excitation (10 V peak to peak) to

10   a contacting piezoelectric transducer (Olympus NDT 500-kHz V101/V151) centred on the sample's end. Coupling between the sample and transducers was ensured by a thin layer of low temperature silicon grease. The resulting oscillations propagate through the ice sample and are detected by another transducer centred on the opposite end of the sample. The transmitted signal is synchronously detected by a DSP Lock-in amplifier (Stanford Research Systems, SR850) and divided into an in-phase component and an out-of-phase component with the reference signal. The magnitude of the two components is recorded

15   on a Tektronix oscilloscope (TDS 3014B) and transferred to a PC via an Ethernet connection.

The sample is mounted in a counter-balanced floating platform (Fig. 2b) to minimize load on the ice by the top transducer, as loading can influence mechanical resonance (Zadler et al., 2004). The apparatus and the sample are placed inside a chest freezer which is allowed to warm slowly from its minimum temperature. To determine sample temperature, an identical ice sample in the same part of the freezer is monitored by a series of thermocouples frozen into its core. The thermocouples are

20   recorded on LabView software using a National Instruments cDAQ thermocouple module equipped with k-type thermocouples. We conducted RUS measurements on ice temperatures between −26°C to −5°C ±0.5°C, sweeping from 5 to 65 kHz.

Travel-time measurements of elastic waves through the long central axis of a warming sample are performed with the same transducers, where an Olympus NDT pulser generates a 200V pulse with a central frequency of 500 kHz. An identical receiving transducer is connected to an oscilloscope to detect the transmitted wave-field.

25   3   Results

3.1   Travel-time measurements

Ultrasonic wave fields allow us to estimate the compressional wave speed V_p as a function of ice temperature (Fig. 3a). The estimated arrival times in Fig. 3b result in $V_p = 3.80 \pm 0.01$ km/s at -25°C. Measurements at successively higher temperatures show that V_p changes -2.2 m/s/°C. The arrival of the secondary (shear) wave is outside the displayed times, but was obscured

30   by scattered compressional waves.

3.2 Resonance measurements

From the observed resonances of our ice core (Fig. 4a), we extract the first 10 resonant frequencies under 40 kHz to estimate the elastic constants as a function of temperature. The resonant frequencies and the associated amplitudes decrease monotonically with increasing ice temperature (Fig. 4b). Subsequent cooling restores the original resonant frequencies and amplitude of the resonance spectra, showing no signs of significant hysteresis. Repeat measurements at fixed temperature give resonant peak positions with a standard deviation of $\sigma^d = 70$ Hz.

For each ice temperature, we invert for the elastic constants by iteratively reducing the misfit, scaled by the data uncertainty as defined in Eq. (5). Iteration is terminated for values of χ^2 between 12 and 14 at each temperature (see Table 1 for the results at $T = -25°$C). From this procedure, we estimate $c_{11} = 12.6 \pm 0.05$ GPa and $c_{44} = 3.6 \pm 0.04$ GPa for standard ice at $T = -25°$C.

The temperature dependence of the elastic properties is captured in Fig. 5a. Values of c_{11} and c_{44} decrease with increasing ice temperature. Estimates of V_p from TOF and RUS in Fig. 5b indicate a difference in absolute value, while both decay monotonically with increasing ice temperature. V_s and c_{44}, however, appear less sensitive to ice temperature than the compressional wave speed and c_{11}.

3.3 Anelasticity

A Matlab curve fitting algorithm (findpeaks.m, from MATLAB, 2016a) detects peaks in the input resonant spectra and the width of the peak at half the maximum amplitude, providing the input to Eq. (6) to estimate the quality factor Q of the ice. While Q generally decreases with increasing temperature (Fig. 6), the temperature dependence of Q for our ice sample presents a bimodal distribution in Q values, and in the sensitivity of Q to temperature. Resonances with overall higher Q values appear more temperature dependent than resonant modes with an overall lower Q.

The Matlab based forward modelling code RUS.m (Fig, 2008) computes the modal shape (torsional, flexural or extensional), associated with each of our observed peaks. Modes with higher overall values of Q – and higher sensitivity to temperature in the ice – are associated with extensional modes (Fig. 6). These modes are essentially an axial compression coupled to a radial expansion (Zadler et al., 2004). Torsional modes, on the other hand, generate rotations of the sample about the vertical axis, depending entirely on the sample's shear velocity. Flexural modes represent energy travelling along paths that are tilted with respect to the sample axis and generate compressional and shear displacements on the end of the sample by bending. We observe extensional modes to be less attenuating, but their attenuation is more temperature dependent than for modes dominated by shear motion (flexural, torsional).

4 Discussion

4.1 Frequency dependence of velocity and attenuation

It is difficult to derive a relationship for the frequency dependence of elastic wave velocity (dispersion) in ice from the literature by using published velocity data measured at different frequencies, as the materials from each experiment are different. Seismic

5 measurements (Kohnen, 1974) represent estimates derived from bulk ice with temperature gradients and significant internal fabric variability. Ultrasonic velocity measurements come from natural samples with variable microstructure (Kohnen and Gow, 1979) or from synthetic bubble free ice with an unknown microstructure (Vogt et al., 2008). Seismic field studies of surface waves (Rayleigh and Love waves) sampling bulk ice with temperature gradients and significant internal fabric variability show strong dispersion at low frequencies (< 100 Hz) (Picotti et al., 2015). However, this type of dispersion results from the sampling

10 of different depths with different frequencies. Long wavelengths sample the deeper (generally faster) ice. Increases in Q with frequency is observed in the laboratory (McCarthy and Cooper, 2016) and in field experiments (Gusmeroli et al., 2010).

Our estimates of V_p from ultrasonic pulsed measurements (10^6 Hz) trend higher than the estimates from RUS at 10^5 Hz (Fig. 5a), and we observe a general increase in Q with increasing frequency for all modal types. Dispersion and attenuation are coupled by the Kramers-Kronig relations (O'Donnell et al., 1981). The observed increase in Q and V_p with frequency is

15 consistent with a visco-elastic medium.

4.2 Temperature dependence and pre-melt

The vertical temperature profile of polar ice sheets is complex. While near surface temperatures are typically below $-20°$C, basal temperatures can approach the bulk melting point (Pattyn, 2010; Cuffey and Paterson, 2010; Engelhardt, 2004; Joughin et al., 2004; Iken et al., 1993). It follows that a significant temperature-induced flow velocity gradient must exist within in an

20 ice body, on top of other contributing factors such as crystalline fabrics, which induce mechanical anisotropy. As a result, the temperature dependence of the elastic properties of ice are of interest from static to ultrasonic frequencies.

The observed temperature dependence in our travel-time estimates of V_p are consistent with Vogt et al. (2008); Kohnen (1974); Bentley (1972, 1971) and Bass et al. (1957). Our results indicate that in the temperature range of interest, the compressional wave speed is more sensitive to temperature than the shear wave speed. Similarly, wave attenuation captured in the

25 quality factor Q exhibits greater temperature sensitivity in the extensional resonant modes.

The quality factor Q for compressional wave dominated extensional modes is greater, and more sensitive to temperature changes, than for flexural and torsional modes associated with shear wave properties. It is well understood that porosity, dislocation structures, the configuration of grain boundaries, and any crystallographic preferred orientation (CPO) textures play an important role in the absolute value of visco-elastic dissipation (McCarthy and Castillo-Rogez, 2013; Cole et al., 1998)

30 and elastic wave speeds (Maurel et al., 2015; Diez and Eisen, 2015; Gusmeroli et al., 2012) in ice, but we attribute pre-melt water films developing on grain boundaries as the dominant mechanism for the changes in the values of the elastic properties and wave attenuation as a function of ice temperature. This has been observed previously by Spetzler and Anderson (1968) and Kuroiwa (1964) in resonant bar measurements and in the field at seismic frequencies (Peters et al., 2012).

5 Conclusions

Laboratory resonance measurements provide quantitative estimates of the temperature dependent elastic properties and wave attenuation of polycrystalline ice. Resonant ultrasound spectroscopy and travel-time measurements reveal wave dispersion and attenuation, as well as the temperature dependence of these properties. The compressional wave speeds and its intrinsic attenuation are most sensitive to temperature, which we attribute to liquid phases on ice grain boundaries associated with pre-melting conditions. Applied to real ice cores, this approach can be used to calibrate sonic logging and seismic field data on ice sheets and glaciers. The RUS method can be deployed in the field, which is important in situations where shipping of ice samples is difficult (e.g. remote locations) or where the properties of ice change rapidly after extraction (e.g., in the case of sea ice).

6 Data availability

The raw resonant ultrasound and travel-time data are freely available on-line through the Auckland University Physical Acoustics Lab website at:

http://www.physics.auckland.ac.nz/research/pal/wp-content/uploads/sites/13 /2016/05/RUS_data_files.zip

Author contributions. MV, DP and KVW conceived the experiments. MV and KVW conducted the experiments. MV and HB processed the data. MV created the figures and wrote the manscript with support from KVW, DP and HB

Acknowledgements. This research was supported by the Marsden Fund of the Royal Society of New Zealand (UOO1116) and a University of Otago Research Grant. MV was supported by a University of Otago postgraduate research scholarship. We thank Jim Woods, Peter Fleury, Leo van Rens and Brent Pooley for ongoing engineering and technical support throughout this project.
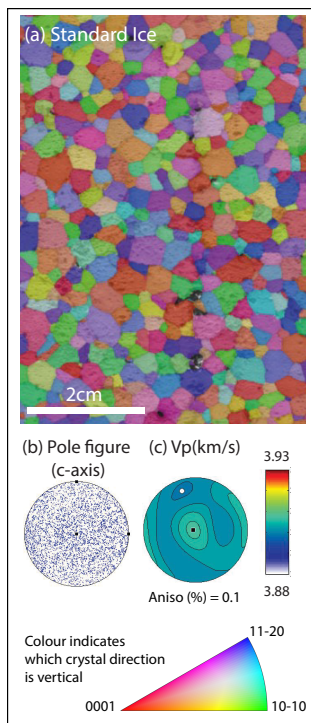
Figure 1. Electron backscatter diffraction (EBSD) data from a sample of standard ice manufactured by the same methods employed for the samples in these experiments. We acquired this map using a Zeiss Sigma VP FEGSEM fitted with on Oxford Instruments Nordlys camera and AZTEC software. Modifications required for cryo-EBSD are described in Prior et al. (2015).(a) EBSD map of standard ice. (b) C-axis pole figure in upper hemisphere projection, indicating the orientation of the c-axis at each pixel.(c) Vp model derived using a Voigt-Reuss-Hill average. The magnitude of anisotropy is indicated (0.1%)
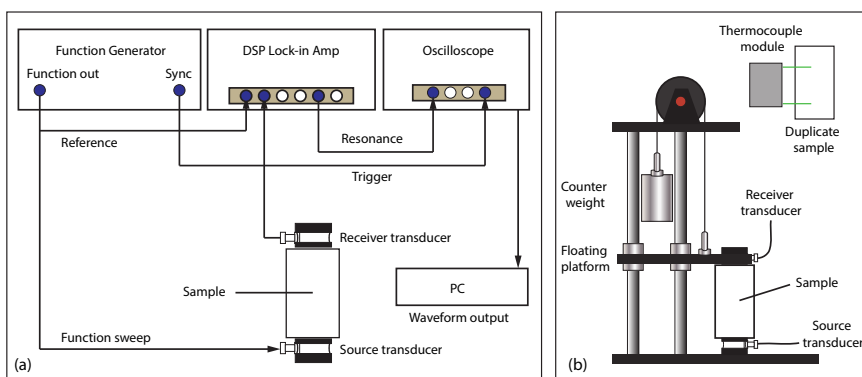
Figure 2. Diagram of the RUS setup (a) and of load-minimizing sample frame with temperature monitoring equipment (b).
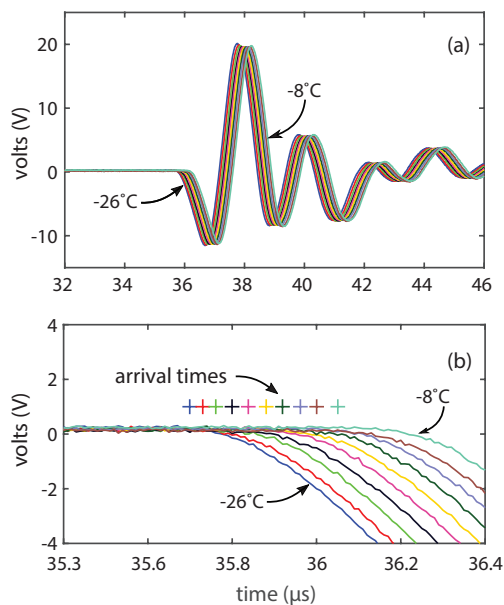
Figure 3. Ultrasonic waveforms, transmitted through our ice cylinder, as a function of temperature (a), with a zoom of the first wave arrival in panel (b).
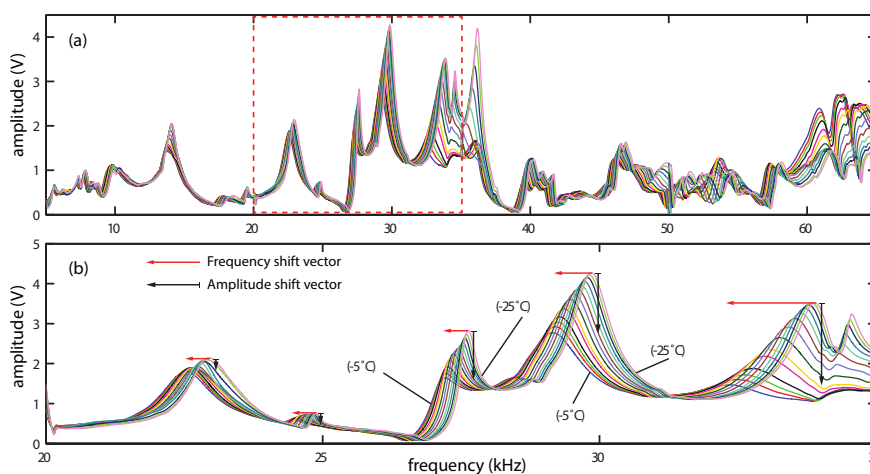
Figure 4. Resonant spectrum of our standard ice sample as a function of temperature (a). The range outlined by the red border is displayed in panel (b).
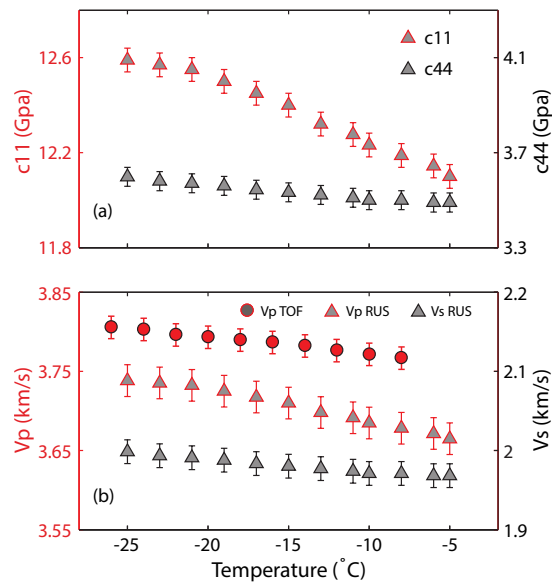
Figure 5. Estimates of the elastic constants c_{11} and c_{44} from RUS as a function of temperature (a). Estimates of V_p and V_s from RUS are compared to V_p estimated from travel-time measurements in panel (b).
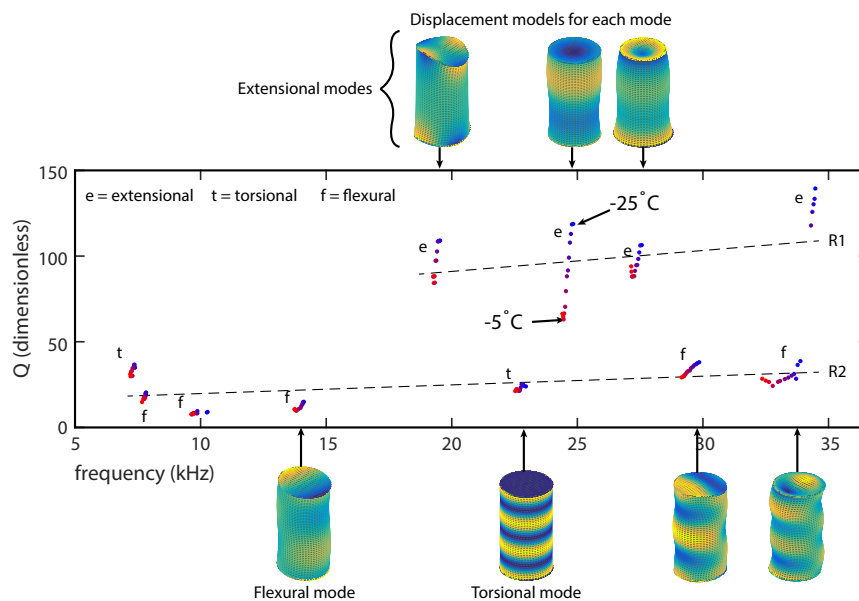
Figure 6. Quality factor Q as a function of temperature and frequency for 11 resonant peaks. Each resonance mode is identified as flexural, extensional or torsional. R1 and R2 are linear regressions for the extensional modes and the flexural/torsional modes respectively, which show a general trend of increasing Q with f.

Table 1. Measured (f^m), initial-model predicted (f_0^p) and final-model predicted (f^p) resonant frequencies for our sample at -25°C. The final column is the relative contribution of each peak to the overall χ^2.

f^m(Hz)	f_0^p(Hz)	f^p(Hz)	$\left(\frac{f^m - f^p}{\sigma^d}\right)^2$
7386	7324	7334	0.55
7830	7334	7363	2.84
10256	11654	11629	76.94
14093	14794	14620	56.68
19583	19664	19580	0.00
22944	22328	22550	31.68
24871	25054	25008	3.83
27624	27893	27855	10.89
29850	29151	29729	2.98
33894	33800	33870	0.05

References

Aki, K. and Richards, P. G.: Quantitative Seismology, 2nd Ed., University Science Books, 2002.

Bass, R., Rossberg, D., and Ziegler, G.: Die elastischen konstanten des Eises, Zeitschrift für Physik, 149, 199–203, 1957.

Bentley, C. R.: Seismic anisotropy in the West Antarctic Ice Sheet, Wiley Online Library, 1971.

5   Bentley, C. R.: Seismic-wave velocities in anisotropic ice: A comparison of measured and calculated values in and around the deep drill hole at Byrd Station, Antarctica, Journal of Geophysical Research, 77, 4406–4420, 1972.

Bentley, C. R. and Kohnen, H.: Seismic refraction measurements of internal-friction in Antarctic ice, Journal of Geophysical Research, 81, 1519–1526, doi:10.1029/JB081i008p01519, <GotoISI>://WOS:A1976BL02700008, 1976.

Cole, D., Johnson, R., and Durell, G.: Cyclic loading and creep response of aligned first-year sea ice, Journal of Geophysical Research: Oceans, 103, 21 751–21 758, 1998.

10   Cuffey, K. M. and Paterson, W. S. B.: The physics of glaciers, Academic Press, 2010.

Diez, A. and Eisen, O.: Seismic wave propagation in anisotropic ice-Part 1:Elasticity tensor and derived quantities from ice-core properties, The Cryosphere, 9, 367–384, 2015.

Durham, W. B., Prieto-Ballesteros, O., Goldsby, D. L., and Kargel, J. S.: Rheological and Thermal Properties of Icy Materials, Space Science Reviews, 153, 273–298, doi:10.1007/s11214-009-9619-1, <GotoISI>://000282381200010, 2010.

15   Duval, P., Ashby, M. F., and Anderman, I.: Rate-controlling processes in the creep of polycrystalline ice, Journal of Physical Chemistry, 87, 4066–4074, <GotoISI>://A1983RM39800014, 1983.

Engelhardt, H.: Thermal regime and dynamics of the West Antarctic Ice Sheet, Annals of Glaciology, 39, 85–92, 2004.

Fig, M.: Resonant Ultrasound Spectroscopy (RUS.m), http://uk.mathworks.com/matlabcentral/fileexchange/ 11399-resonant-ultrasound-spectroscopy--rus-, 2008.

20   Gammon, P., Kiefte, H., and Clouter, M.: Elastic constants of ice samples by Brillouin spectroscopy, The Journal of Physical Chemistry, 87, 4025–4029, 1983.

Gribb, T. T. and Cooper, R. F.: Low-frequency shear attenuation in polycrystalline olivine: Grain boundary diffusion and the physical significance of the Andrade model for viscoelastic rheology, Journal of Geophysical Research-Solid Earth, 103, 27 267–27 279, 25   <GotoISI>://000076918900025, 1998.

Gusmeroli, A., Clark, R. A., Murray, T., Booth, A. D., Kulessa, B., and Barrett, B. E.: Seismic wave attenuation in the uppermost glacier ice of Storglaciaren, Sweden, Journal of Glaciology, 56, 249–256, <GotoISI>://WOS:000280258200006, 2010.

Gusmeroli, A., Pettit, E. C., Kennedy, J. H., and Ritz, C.: The crystal fabric of ice from full-waveform borehole sonic logging, Journal of Geophysical Research: Earth Surface, 117, 2012.

30   Hobbs, P. V.: Ice physics, Oxford University Press, Oxford, 1974.

Hooke, R. L., Mellor, M., Budd, W. F., Glen, J. W., Higashi, A., Jacka, T. H., Jones, S. J., Lile, R. C., Martin, R. T., Meier, M. F., Russellhead, D. S., and Weertman, J.: Mechanical properties of polycrystalline ice - An assesment of current knowledge and priorities for research - Report prepared for the Internation Commission on Snow and Ice, with support from the United States Science Foundation, Cold Regions Science and Technology, 3, 263–275, <GotoISI>://A1980KE96800001, 1980.

35   Horgan, H. J., Anandakrishnan, S., Alley, R. B., Peters, L. E., Tsoflias, G. P., Voigt, D. E., and Winberry, J. P.: Complex fabric development revealed by englacial seismic reflectivity: Jakobshavn Isbræ, Greenland, Geophysical Research Letters, 35, doi:L1050110.1029/2008gl033712, <GotoISI>://WOS:000256137500005, 2008.

Horgan, H. J., Anandakrishnan, S., Alley, R. B., Burkett, P. G., and Peters, L. E.: Englacial seismic reflectivity: Imaging crystal-orientation fabric in West Antarctica, Journal of Glaciology, 57, 639–650, <GotoISI>://WOS:000295019400006, 2011.

Iken, A., Echelmeyer, K., Harrison, W., and Funk, M.: Mechanisms of fast flow in Jakobshavns Isbræ, West Greenland. I: Measurements of temperature and water level in deep boreholes, Journal of Glaciology, 39, 15–25, 1993.

5 Jackson, I., Fitz Gerald, J. D., Faul, U. H., and Tan, B. H.: Grain-size-sensitive seismic wave attenuation in polycrystalline olivine, Journal of Geophysical Research-Solid Earth, 107, art. no.–2360, <GotoISI>://000181225600001, 2002.

Joughin, I., Tulaczyk, S., MacAyeal, D. R., and Engelhardt, H.: Melting and freezing beneath the Ross Ice Streams, Antarctica, Journal of Glaciology, 50, 96–108, 2004.

Kohnen, H.: The temperature dependence of seismic waves in ice, J. Glaciol, 13, 144–147, 1974.

10 Kohnen, H. and Gow, A. J.: Ultrasonic velocity investigations of crystal anisotropy in deep ice cores from Antarctica, Journal of Geophysical Research: Oceans, 84, 4865–4874, 1979.

Kuroiwa, D.: Internal Friction of Ice. I; The Internal Friction of H_2O and D_2O Ice, and the Influence of Chemical Impurities on Mechanical Damping, Contributions from the Institute of Low Temperature Science, 18, 1–37, 1964.

Kuroiwa, D. and Yamaji, K.: Internal friction in polycrystalline and single-crystal ice, Contrib. Inst. Low Temp. Sci. Hokkaido Univ., Ser. A,, 18, 1959.

15 Liefferinge, B. V. and Pattyn, F.: Using ice-flow models to evaluate potential sites of million year-old ice in Antarctica, Climate of the Past, 9, 2335–2345, 2013.

MATLAB: version 9.0.0.34, signal processing toolbox, The MathWorks Inc., Natick, Massachusetts, 2016a.

Matsushima, J., Suzuki, M., Kato, Y., Nibe, T., and Rokugawa, S.: Laboratory experiments on compressional ultrasonic wave attenuation in
20 partially frozen brines, Geophysics, 73, N9–N18, 2008.

Maurel, A., Lund, F., and Montagnat, M.: Propagation of elastic waves through textured polycrystals: Application to ice, in: Proceedings of the Royal Society of London A: Mathematical, Physical and Engineering Sciences, vol. 471, p. 20140988, The Royal Society, 2015.

McCarthy, C. and Castillo-Rogez, J. C.: Planetary ices attenuation properties, in: The Science of Solar System Ices, pp. 183–225, Springer, 2013.

25 McCarthy, C. and Cooper, R. F.: Tidal dissipation in creeping ice and the thermal evolution of Europa, Earth and Planetary Science Letters, 443, 185–194, 2016.

McCarthy, C., Takei, Y., and Hiraga, T.: Experimental study of attenuation and dispersion over a broad frequency range: 2. The universal scaling of polycrystalline materials, Journal Of Geophysical Research-Solid Earth, 116, doi:B09207 10.1029/2011jb008384, <GotoISI>://WOS:000295520900001, 2011.

30 O'Donnell, M., Jaynes, E. T., and Miller, J. G.: Kramers–Kronig relationship between ultrasonic attenuation and phase velocity, The Journal of the Acoustical Society of America, 69, 696–701, doi:http://dx.doi.org/10.1121/1.385566, http://scitation.aip.org/content/asa/journal/jasa/69/3/10.1121/1.385566, 1981.

Pattyn, F.: Antarctic subglacial conditions inferred from a hybrid ice sheet/ice stream model, Earth and Planetary Science Letters, 295, 451–461, 2010.

35 Peters, L. E., Anandakrishnan, S., Alley, R. B., and Voigt, D. E.: Seismic attenuation in glacial ice: A proxy for englacial temperature, Journal of Geophysical Research-Earth Surface, 117, doi:F02008 10.1029/2011jf002201, <GotoISI>://WOS:000302896500002, 2012.

Picotti, S., Vuan, A., Carcione, J. M., Horgan, H. J., and Anandakrishnan, S.: Anisotropy and crystalline fabric of Whillans Ice Stream (West Antarctica) inferred from multicomponent seismic data, Journal of Geophysical Research-Solid Earth, 120, 4237–4262, doi:10.1002/2014jb011591, <GotoISI>://WOS:000357993000014, 2015.

Prior, D., Lilly, K., Seidemann, M., Vaughan, M., Becroft, L., Easingwood, R., Diebold, S., Obbard, R., Daghlian, C., Baker, I., et al.: Making
5   EBSD on water ice routine, Journal of microscopy, 259, 237–256, 2015.

Spetzler, H. and Anderson, D. L.: The effect of temperature and partial melting on velocity and attenuation in a simple binary system, Journal of Geophysical Research, 73, 6051–6060, 1968.

Stern, L. A., Durham, W. B., and Kirby, S. H.: Grain-size-induced weakening of H2O ices I and II and associated anisotropic recrystallization, Journal of Geophysical Research: Solid Earth, 102, 5313–5325, 1997.

10 Vogt, C., Laihem, K., and Wiebusch, C.: Speed of sound in bubble-free ice, The Journal of the Acoustical Society of America, 124, 3613–3618, 2008.

Watson, L. and van Wijk, K.: Resonant ultrasound spectroscopy of horizontal transversely isotropic samples, Journal of Geophysical Research-Solid Earth, 120, 4887–4897, <GotoISI>://WOS:000359746700013, 2015.

Zadler, B. J., Le Rousseau, J. H. L., Scales, J. A., and Smith, M. L.: Resonant ultrasound spectroscopy: Theory and application, Geophysics
15 Journal International, 156, 154–169, doi:10.1111/j.1365-246X.2004.02093.x, 2004.